Magnetic Vortex Dynamics Using the Optical Cotton-Mouton Effect

B. E. Argyle, E. Terrenzio,[a] and J. C. Slonczewski
IBM T. J. Watson Research Center, Yorktown Heights, New York 10598
(Received 9 April 1984)

The first use of linear magnetic birefringence (optical Cotton-Mouton effect) to observe a magnetic resonance is reported. This allows us to make the first direct observation of resonant motion of a ferromagnetic vortex. This vortex is present in an easy-plane garnet film at the intersection of two 90° Néel walls. Agreement between the resonant frequencies and our theory confirms a previously proposed equation of vortex motion.

PACS numbers: 76.90.+d, 75.40.Dy, 76.50.+g, 78.20.Ls

We present here the first conclusive evidence for a Magnus-type force acting on a simple, topologically quantized vortex in a ferromagnetic medium. The existence of such forces which act orthogonally to the velocity of quantized superfluid and superconducting vortices is well known. A similar force, based on the classical Landau-Lifshitz equation that describes ferromagnetic-spin precessions, is expected to act on vortices occurring in a ferromagnet.[1] It illustrates a general law stating that the effective force component orthogonal to the velocity $\vec{V}$ of a micromagnetic structure (soliton) $\vec{M}(\vec{x}-\vec{V}t)$ is proportional to the product of V and the spherical angle mapped by the structure's distribution in $\vec{M}$ space.[2] This force is dominant whenever pseudoinertial effects can be neglected.[3]

Recent unpublished work provides evidence of a resonance provisionally attributed to the motion of a magnetic vortex present within a Bloch line in a 180° Néel wall found in a garnet film of 0.8 μm thickness.[4] This configuration was complicated by the absence of a well-defined restoring force for the wall due to the presence of permeable closure domains at its ends. However, these results did give some support to the equation of vortex motion employed in a statistical theory of two-dimensional ferromagnetism.[1]

We have now investigated the dynamics of a magnetic vortex which forms at the intersection of two 90° Néel walls separating well defined in-plane domains stabilized by a "Swiss cross" geometry (Fig. 1). In this geometry, fixing the four-ends of the walls to the inner corners defines the restoring force. Moreover, the walls do not touch closure domains. Thus the present configuration is suitable for a conclusive comparison of experiment with theory.

Figure 2(a) shows a magneto-optic photomicrograph of two static 90° Néel walls intersecting at right angles. The bright or dark contrast of the walls is obtained by means of the Cotton-Mouton effect, a linear birefringence, $\Delta n = n_{\parallel} - n_{\perp}$, for the two eigenmodes of linearly polarized light, parallel and perpendicular to the magnetization. (The circular birefringence or Faraday effect is absent because the in-plane magnetization is orthogonal to the normally incident laser illumination.) Intensity contrast between regions of different orientations of $\vec{M}_{xy}$ becomes visible when an optical compensator and an analyzer are suitably adjusted. (We utilize an adjustable Ehringhaus compensator with its axes fixed at 45° with respect to the crossed polarizer and analyzer axes.) For incident y-polarized light $\vec{E} = E_y\hat{y}$, the transmitted light contains not only $E_y' = E_y e^{i\bar{\psi}}$, where $\bar{\psi} = 2\pi h(n_{\parallel} + n_{\perp})/2\lambda_0$ is the normal phase shift (neglecting absorption), but also

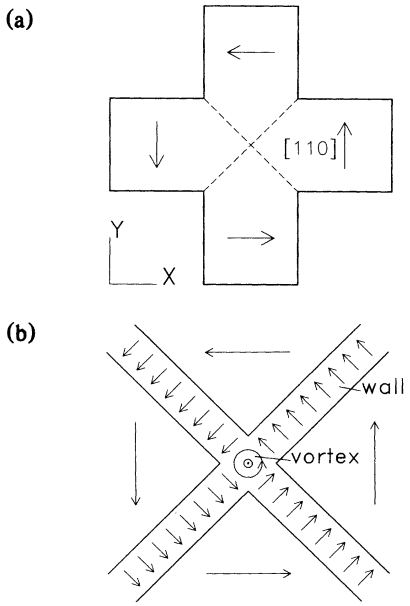

FIG. 1. Schematic illustrations of (a) magnetic film containing a pair of intersecting 90° domain walls, and (b) central detail of the continuous micromagnetic distribution. Generally $\vec{M}$ lies parallel to the film plane, except within the vortex region on whose axis it lies normal to the plane.

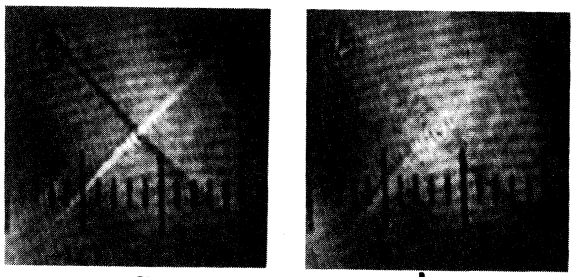

FIG. 2. Photomicrographs of intersecting walls in (a) static and (b) excited resonant oscillation. Wall contrast is due to the optical Cotton-Mouton effect. (See text.) The scale is one micron per division.

an out-of-plane x-component[5]

$$E_x' = E_y e^{i\bar{\psi}} \sin 2\theta \sin\Delta\psi e^{i\pi/2}, \quad (1)$$

where $\theta = \arctan(-M_x/M_y)$. The factor $\sin 2\theta$ reflects a quadratic dependence of the dielectric tensor on the components of $\vec{M}$, rather than linear as in the case of circular birefringence. The amplitude of E_x' as measured by the coefficient $\Delta\psi = 2\pi\Delta nh/2\lambda_0 = 3\times10^{-4}$ is correspondingly smaller by one to two orders of magnitude. The transmitted elliptical light, $E_x'\hat{x} + E_y'\hat{y}$, is right- or left-handed depending on the quadrant of $\vec{M}_{xy}$, i.e., on the sign of $\sin 2\theta$ in Eq. (1). The compensator setting for best contrast occurs when elliptical light of one sense is converted to linear, thus allowing a dark region to occur by extinction with the analyzer. The elliptic light of opposite sense, i.e., arising from a region with $\vec{M}_{xy}$ in the adjacent quadrant, becomes more nearly circular, thus producing a bright region by its partial transparency through the analyzer.

The wall contrast in Fig. 2 is bright or dark depending on the wall-magnetization orientation and the sign of the retardation due to the compensator. The bright walls in Fig. 2 have $\vec{M}_{xy}$ at $\theta = 45°$ and 225° with respect to incident light $E_y\hat{y}$ while the dark walls are at 135° and 315°. Contrast between *domains* is absent in Fig. 2 because $\sin 2\theta = 0$ for domains both parallel and perpendicular to the incident $E_y\hat{y}$. Hence, the analyzer along $\hat{x}$ removes this light although some background light due to imperfections in the analyzer, the microscope, and the TV camera is recorded. The curved striations are due to optical interference effects in the camera.

Our Néel walls occur in 0.8-μm-thick garnet films grown epitaxially with composition $Eu_{0.7}Tm_{0.5}$-$Ga_{0.85}$:(yttrium iron garnet) on a (100) substrate of $Gd_3Ga_5O_{12}$.[4,5] A growth anisotropy mechanism produces strongly negative uniaxial anisotropy ($K_u = -4\times10^4$ erg/cm^3) forcing the spontaneous magnetization ($M_s = 30$ G) to lie in the film plane. The fact that a Néel wall (with $\vec{M}$ in the film plane) has lower energy than a Bloch wall (with $\vec{M}$ in the wall plane) was already discussed in connection with a garnet film having properties very similar to ours.[6]

Magnetocrystalline anisotropy ($K_1 = -6\times10^3$ erg/cm^3) produces easy directions of magnetization along [110] axes. The four [110] domains in Fig. 1(a) are stabilized additionally by the straight [110] boundaries of the "Swiss cross" pattern created by implanting He^{2+} ions through a mask to destroy the magnetization outside the pattern. The four ends of the walls are fixed at the inside corners of the cross.

Although it is too small to be resolved, we conclude by a continuity argument that at the center of the wall junction there is present a vortex structure of a type well known theoretically[7] but never directly by experiment. Consider a circuit in the form of a circle centered at the junction. If the radius R is large compared both to the optical resolution limit and to the wall thickness $\Delta = 2^{-1}\pi(A/|K_1|)^{1/2} \simeq 1000$ Å,[8] our microscope contrast reveals a pattern of magnetic vectors whose angle θ increases by 2π. Then, by continuity, on a circle with $R < \Delta$, θ must also increase by 2π as illustrated in Fig. 1(b). In addition, theoretically,[7] the spins deviate from the film xy plane within a radius $(A/|K_u|)^{1/2}$ of the vortex core, which in our case (with $A = 2\times10^{-7}$ erg/cm), amounts to about 200 Å. At the vortex center only a film-normal component $M_z = \pm M_s$ is present. With increasing distance from the center $\vec{M}$ tilts and develops an increasing azimuthal component to give the circulation about the axis.

The vortex and wall positions are modulated by external in-plane fields. Oscillations are viewed with an oil-immersion 100× 1.3 numerical aperture objective and electronically detected,[9] while the in-plane field is slowly swept in frequency. Figure 2(b) shows blurring of the image when the motion is driven at resonance by a sinusoidal field of amplitude ~2 Oe (peak). The observed resonances for three different pattern sizes making wall lengths $L = 14$, 28, and 35 μm occur at 24, 15.5, and 13 MHz, respectively. However, the large amplitudes (> 1 Oe peak) necessary for visual detection in the blurred image are in a nonlinear response regime. This is shown by swept frequency response curves (Fig. 3) obtained photometrically with photomultiplier tube detection and a microspot aperture.[9] The natural resonance frequency (30 MHz) occurring for $L = 14$ μm at low drive (below 1 Oe peak) is somewhat above the 24 MHz seen visually (~2 Oe

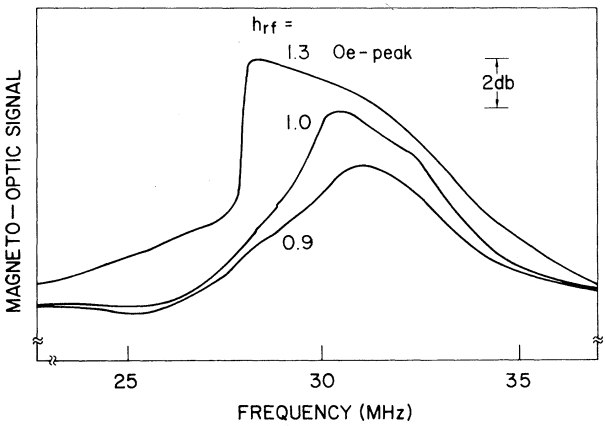

FIG. 3. Photometric resonance spectrum for wall length $L = 14$ μm obtained with a microspot aperture (~ 0.5 μm) asymmetrically located with respect to the wall coupled to the vortex.

peak), where nonlinear response is so prominently evidenced by the asymmetric line shape. An additional unique feature is that the motion of the vortex at resonance appears to be circular regardless of the direction of the in-plane rf field.

If we let the complex notation $\xi = \xi' + i\xi''$ indicate the Cartesian position (ξ', ξ'') of the vortex, the equation of vortex motion[1] in linearized form is

$$\pm 2\pi i h M_s \gamma^{-1} \, d\xi/dt = W''\xi, \tag{2}$$

where h is the film thickness, M_s is the spontaneous magnetization, γ is the gyromagnetic ratio, and the restoring force coefficient $W'' = (d^2W/d\xi^2)_{\xi=0}$ is derived from the total energy W of the system. The left-hand side of Eq. (2) represents the general gyrotropic force $F = hM_s\Omega V/\gamma$ orthogonal to the velocity $\vec{V}$.[1-3] Here $\Omega = \pm 2\pi$ is the spherical angle mapped by the vortex. The choice of plus or minus depends on the sign of M_z within the vortex core. Solving Eq. (2) gives the frequency of natural resonance,

$$\nu = \gamma W''/(2\pi)^2 h M_s \tag{3}$$

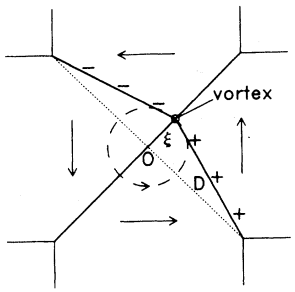

FIG. 4. Idealized displacement of a 90° wall coupled to the vortex. The resonant orbit of the vortex is indicated by the dashed circle.

at which the vortex executes a circular orbit $\xi = \xi_0 e^{\pm 2\pi i \nu t}$.

We approximate W with the stray-field energy which arises when the walls are displaced from equilibrium. (The changes in exchange and anisotropy were found to be negligibly small.) The stray fields originate from the extra magnetic poles due to the net change of the wall-normal component of $\vec{M}$ across the wall (see Fig. 4). The length $D = L/2$ of each 90° wall segment is much greater than the thickness $h = 0.8$ μm of the film. Therefore, we regard the poles $\rho(x)$ as distributed on lines s representing dynamic wall positions. Thus, the energy is

$$W = \frac{1}{2}\int\int \frac{\rho(\vec{x}_1)\rho(\vec{x}_2)\,ds_1\,ds_2}{(|\vec{x}_1 - \vec{x}_2|^2 + a^2)^{1/2}}. \tag{4}$$

The constant a (> 0), inserted arbitrarily, serves to eliminate the singularity at $\vec{x}_1 = \vec{x}_2$ in the above integration. Comparing Eq. (4) with the closed-form-integrable case of a long uniformly charged strip of width h, one finds $a = e^{3/2}h$. Since ρ varies slowly over the length of our wall, we may also use this expression for a in Eq. (4).

To estimate W explicitly, we idealize the generally curved dynamically displaced wall with two straight segments of length $D = L/2$ as shown in Fig. 4. For small ξ the line-charge density is now $\rho = \pm\sqrt{2}M_s h\xi/D$ and Eq. (4) becomes

$$W = 2(hM_s\xi/D)^2 \int_0^D dx_1 \int_0^D dx_2 \{[a^2 + (x_1 - x_2)^2]^{-1/2} - [a^2 + (x_1 + x_2)^2]^{-1/2}\}. \tag{5}$$

The first term in the integrand provides the sum of self-interactions of the separate displaced segments, while the second provides the interaction *between* them. From standard tables of integrals one finds

$$W'' = M_s^2 h^2 D^{-1}[12 + 8\ln(D/h)] \quad (h/D \ll 1). \tag{6}$$

We employ the measured thickness $h = 0.8$ μm and the material parameters $M_s = 30$ G and $\gamma = -1.36 \times 10^7$ sec^{-1} Oe^{-1} estimated from measurements on similar compositions. Equations (3) and (6) give $\nu = 34$, 20, and 17 MHz respectively, for the three values of $L = 2D$ of the experiment. These are some 13% ot 30% greater than our experimental frequencies. Much of this discrepancy appears due to the nonlinear shift exhibited in Fig. 3.

The remainder may be attributed to our neglect of wall bowing and of stray fields due to fixed poles distributed along the edges of the film geometry.

One can show that the areal density of 90° Néel-wall effective mass[10] $M_s^2|K_1|^{1/2}/2A^{1/2}|K_u|\gamma^2$, whose effect we have neglected, contributes negligibly to the resonant frequency. Thus, one can say that the resonant motion in this experiment essentially involves precessions of just those electron spins within the invisibly small vortex-core region carrying a film-normal flux on the order of 0.03 times the superconducting flux quantum $ch/2e = 2.07\times10^{-7}$ G cm^2.

We are grateful to E. A. Giess and C. F. Guerci who grew the film, G. E. Keefe who made the ion-implantation pattern, and R. E. Mundie for valuable technical assistance.

---

[a]Present address: Istituto di Fisica, Università Degli Studi dell'Aquila, 67100 L'Aquila, Italy.

[1]D. L. Huber, J. Appl. Phys. **53**, 1899 (1982).

[2]A. A. Thiele, Phys. Rev. Lett. **30**, 230 (1973).

[3]J. C. Slonczewski, J. Magn. Magn. Mater. **12**, 108 (1979).

[4]B. E. Argyle, M. H. Kryder, G. E. Keefe, and J. C. Slonczewski, in Proceedings of the 1983 Intermag Conference, Pittsburgh, April 1983 (to be published).

[5]B. E. Argyle and E. Terrenzio, J. Appl. Phys. **55**, 2569 (1984).

[6]M. H. Kryder, T. J. Gallagher, and R. A. Scranton, J. Appl. Phys. **53**, 5810 (1982).

[7]S. Hikami and T. Tsuneto, Prog. Theor. Phys. **63**, 387 (1980).

[8]For small M_s, the effect of demagnetization on the thickness of a 180° wall is profound [see J. C. Slonczewski, J. Appl. Phys. **55**, 2536 (1984)]. However, since its effect on a 90° wall is small, we have neglected it in this expression for wall thickness.

[9]B. E. Argyle, W. Jantz, and J. C. Slonczewski, J. Appl. Phys. **54**, 3370 (1983).

[10]Slonczewski, Ref. 8.

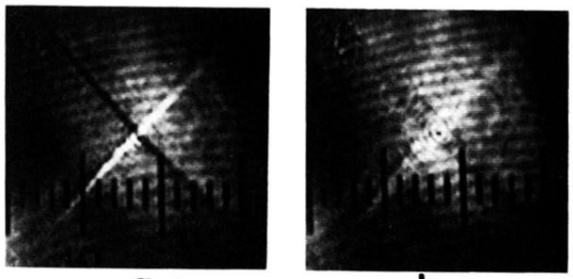

FIG. 2. Photomicrographs of intersecting walls in (a) static and (b) excited resonant oscillation. Wall contrast is due to the optical Cotton-Mouton effect. (See text.) The scale is one micron per division.